Torque Prediction Using the Flux-MMF Diagram in AC, DC, and Reluctance Motors

David A. Staton, Rajesh P. Deodhar, *Student Member, IEEE,* Wen L. Soong, *Member, IEEE,* and Timothy J. E. Miller, *Senior Member, IEEE*

***Abstract*—This paper uses the flux-MMF diagram to compare and contrast the torque production mechanism in seven common types of electric motor. The flux-mmf diagram is a generalized version of the flux-linkage versus current (ψ-i) diagram for switched-reluctance motors. It is illustrated for switched-reluctance, synchronous-reluctance, induction, brushless ac, brushless dc, interior PM and dc commutator motors. The calculated flux-MMF diagrams for motors with the same electromagnetic volume, airgap, slotfill, and total copper loss are shown and are used to compare the low-speed torque and torque ripple performance. The motor designs used were reasonably optimized using a combination of commercially available motor CAD packages and finite-element analysis.**

I. Introduction

THE FLUX-LINKAGE versus current (ψ-i) diagram has traditionally been used to analyze the switched-reluctance motor (SRM) performance characteristics [1]–[6]. Recently this concept has been extended to synchronous-reluctance (SYNCHREL) motors [5] and doubly salient permanent magnet (DSPM) motors [6] in order to facilitate a direct comparison with the SRM. The concept of electromagnetic torque being derived from the (ψ-i) characteristics is however fundamental to all electric motors [7]–[9]. This paper shows how the flux-MMF diagram can be derived from the (ψ-i) diagram and applied to several motor types, providing a unified method of analysis and evaluation.

Section II describes the salient features of the flux-MMF diagram and gives the relevant definitions of flux and MMF. Section III explains the constraints applied in designing the seven motor types used in the comparison. Section IV describes the flux-MMF diagram of each motor. Finally Section V compares and contrasts the seven motor types.

II. The Flux-MMF Diagram

The ψ-i diagram is based on plotting the variation of instantaneous phase flux-linkage against the instantaneous phase current. The *instantaneous torque* per phase is given by [1]–[3]

$$T = \left.\frac{\partial W'(i,\theta)}{\partial \theta}\right|_{i=constant} \tag{1}$$

where W' is the *co-energy*, i is the instantaneous phase current and θ is the rotor position. The partial differentiation is performed by dividing the area enclosed between two successive magnetization curves by the rotor displacement. The *average electromagnetic torque* per phase is proportional to the area enclosed by the ψ-i locus over one electrical cycle. Thus

$$T_{AV} = \frac{mp}{2\pi} \times W' \tag{2}$$

where W' is the energy converted as shown in Fig. 1, m is the number of phases and p is the number of pole-pairs.

To eliminate the arbitrariness of the number of turns from the analysis, the phase flux-linkage and current are respectively divided and multiplied by $N_{\rm ph}$, the series turns/phase, to give the "effective" phase flux and phase MMF. These are similar to per-unit quantities. The quantity $\psi/N_{\rm ph}$ is not the actual flux in the machine but the *effective flux* which links the winding and thus produces torque. The converted energy can be calculated from either the flux-MMF or ψ-i locus, since both enclose the same area as shown in Fig. 1. The flux-MMF diagram is independent of the particular voltage level for which the motor happens to be wound. The important features of the flux-MMF diagram are the following:

- Area enclosed indicates torque capability.
- Shape indicates nature of excitation (ideally ellipsoidal for sinewave and rectangular for squarewave).
- Deviation from ideal shape and uneven spacing of magnetization curves indicates torque ripple and saturation.
- Whereas d-q axis theory can only predict average torque, this method can predict torque ripple as well.
- Orientation of the major axis with respect to the MMF-axis indicates the kVA utilization (power factor in sinewave motors).
- Electric and magnetic loadings and their utilization are indicated graphically.

The flux-MMF diagram for a particular motor is shown with *magnetization curves* superimposed (e.g., Figs. 5 and 12). These are generated using a series of static finite-element analyses at incremental rotor positions (θ) and increasing loads.

The method of predicting torque ripple using the ψ-i diagram has been validated for synchronous reluctance motors

Paper IPCSD 95–53, approved by the Electric Machines Committee of the IEEE Industry Applications Society for presentation at the 1994 Industry Applications Society Annual Meeting, Denver, CO, October 2–7. Manuscript released for publication July 11, 1995.

D. A. Staton is with Control Techniques plc, Newtown, Wales SY16 3AJ, U.K.

R. P. Deodhar and T. J. E. Miller are with the SPEED Laboratory, University of Glasgow, U.K.

W. L. Soong is with the GE Corporate Research and Development, Schenectady, NY 12301 USA.

Publisher Item Identifier S 0093-9994(96)00322-2.

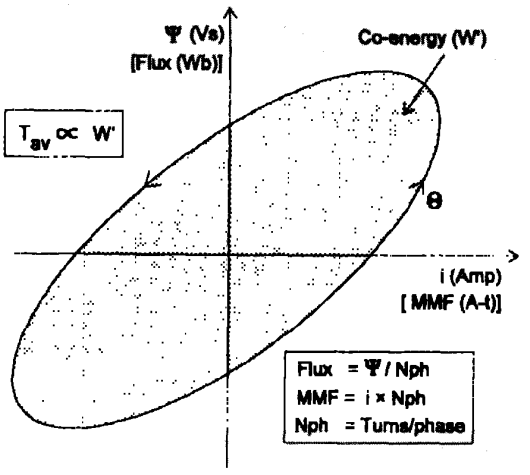

Fig. 1. The equivalence between the ψ-i and flux-MMF diagrams.

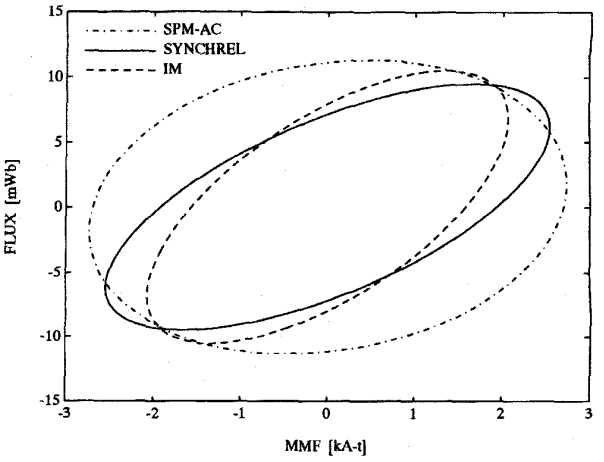

Fig. 2. flux-MMF diagram for the IM, SYNCHREL and SPM-AC motors (full-load).

TABLE I
DESIGN CONSTRAINTS

Parameter	Constraint
Stator outer diameter	8 inches (203.2mm)
Active length	8 inches (203.2mm)
Airgap	0.5mm
Slot fill	40%
Copper loss	634W

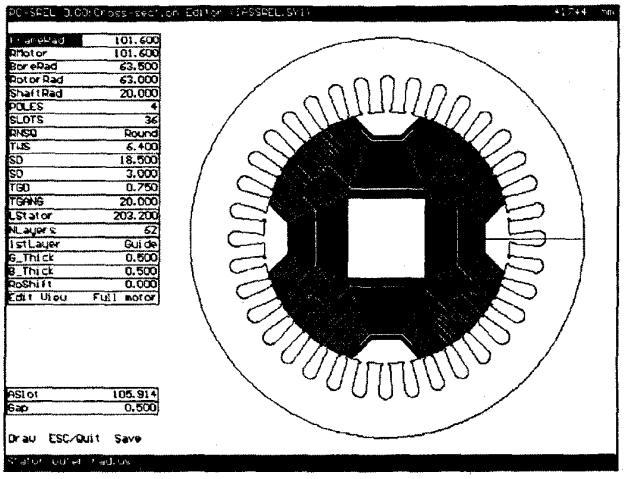

Fig. 3. SYNCHREL motor design.

with measurements as shown in Figs. 5 and 6 [5]. In the interest of simplicity this paper presents only the electromagnetic torque and neglects *cogging*, which contributes no useful average torque. However, it is possible to calculate the cogging torque using the flux-MMF diagram technique [10]. Briefly, this is done by calculating the variation in magnet working point with rotation. The flux-MMF diagram is then constructed using the demagnetization characteristic.

III. DESIGN CONSTRAINTS

A standard D132 frame induction motor (Section IV-A) has been used as the basis for designing all the motors used in this comparison. Each has the same electromagnetic volume, airgap, slot-fill, and total copper loss (at 115°C and 7.5 kW rating) as the induction motor (Table I). Friction, windage, and iron losses are not quoted here, so that the conclusions made from the comparison are strictly valid at low speed.

IV. MOTORS USED IN THE COMPARISON

A. Induction Motor (IM)

This is a standard D132 induction motor, capable of 11 kW when operated from a 50-Hz sinusoidal supply. It must be derated to 7.5 kW for operation from a variable speed supply (10 : 1 speed ratio) with constant torque (50 Nm). The total copper loss at the 7.5 kW rating is equal to 634 W (stator copper loss = 426 W; rotor copper loss = 208 W); this is the main design constraint used in the comparison.

The flux-MMF diagram for the IM is derived from the phasor diagram. The instantaneous voltage and current is given by

$$i = \hat{I}\cos(\omega t - \phi); \qquad v = \hat{V}\cos(\omega t).$$

The flux-linkage is calculated using

$$\lambda = \int v\,dt = \hat{V}/\omega \sin(\omega t).$$

The flux-MMF diagram for the IM at full-load is shown together with that of the SYNCHREL (Section IV-B) and SPM-AC (Section IV-D) motors in Fig. 2.

B. Synchronous Reluctance Motor (SYNCHREL)

An axially laminated rotor is used in the comparison since it has been shown that this construction gives the maximum

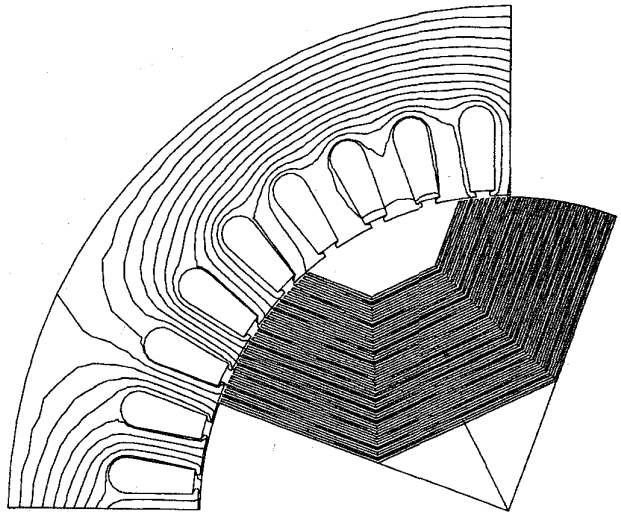

Fig. 4. SYNCHREL flux-plot (full-load, $\theta = 20°, \gamma = 60°$).

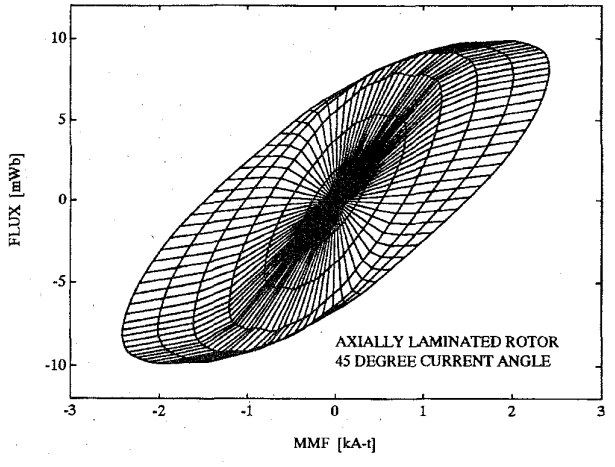

Fig. 5. Flux-MMF diagram and magnetization curves for the SYNCHREL motor (6 phase current values with the maximum at full-load).

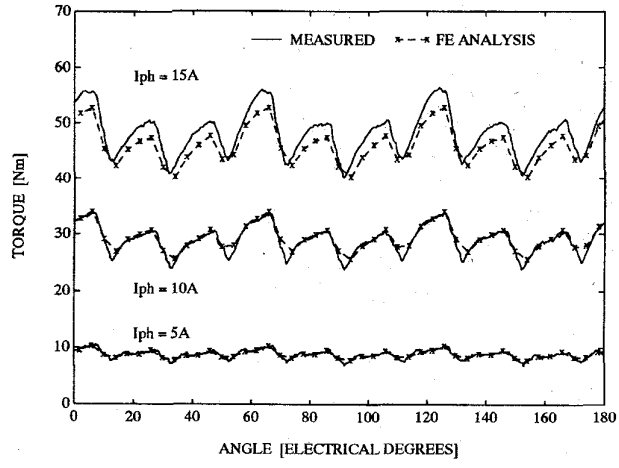

Fig. 6. SYNCHREL measured and calculated (FE analysis) torque-ripple.

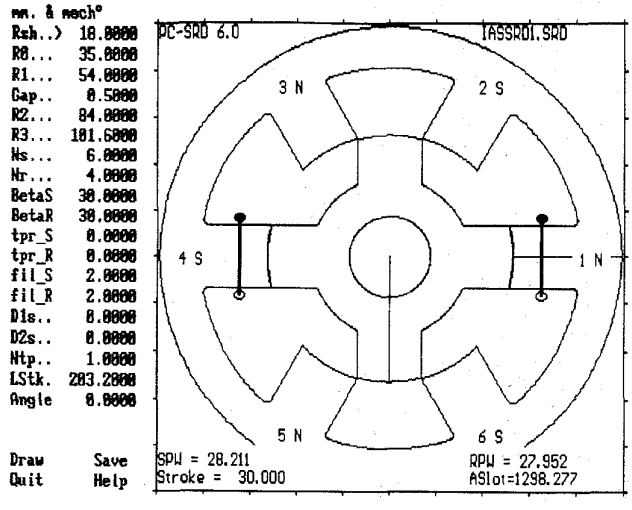

Fig. 7. SRM design.

saliency ratio [11]–[20]. The stator and winding type are the same as used in the induction motor. The motor cross section is shown in Fig. 3. This is a screen-capture taken from a synchronous reluctance motor design program *(PC-SREL)*. An on-load flux plot taken from the finite-element analysis is shown in Fig. 4. The predicted flux-MMF diagram is shown in Fig. 5 and the torque waveform in Fig. 6. The angle γ between the stator MMF axis and the rotor q-axis (high-inductance axis) is set at 60° to give maximum torque/ampere under saturated conditions [12].

C. Switched Reluctance Motor (SRM)

The calculation of SRM torque from the ψ-i locus is well documented [1]-[3]. The 6:4 SRM used in this analysis was designed using the *PC-SRD* program [1], [3], [22] and is shown in Fig. 7. It has the same number of phases and energy conversion strokes per revolution as the other brushless motors used in the comparison. The 6:4 motor has high torque ripple as shown in Fig. 8. Fig. 9 compares the flux-MMF diagram at full-load with that of the SYNCHREL motor (Section V-B).

D. Surface Permanent Magnet Brushless AC (SPM-AC)

The surface permanent magnet brushless ac (SPM-AC) motor used in the analysis is shown in Fig. 10. It was designed using the *PC-BDC* program [21], [22]. It has rare-earth magnets with a remanence of 1.1 T to give flux-density levels comparable to those in the IM. The magnet arc and distributed winding configuration were selected to give a sinusoidal back-emf.

Fig. 12 plots the flux-MMF diagram (with magnetization curves) at 6 currents ranging from no-load to full-load. The dynamic locus of the operating point (whose coordinates are MMF and effective flux) is nearly elliptical. The magnetization curves are virtually straight because the flux-linkage is set by the magnets and is virtually independent of the current. Slight irregularities in the otherwise regular spacing of the magnetization curves indicate a small amount of torque ripple

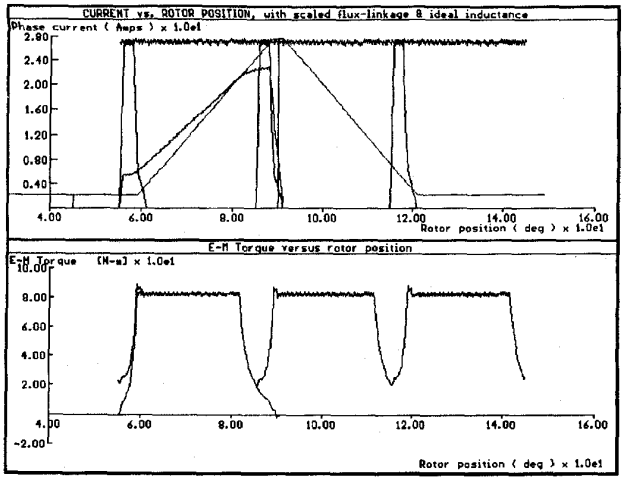

Fig. 8. SRM phase current and torque waveforms (150 r/min).

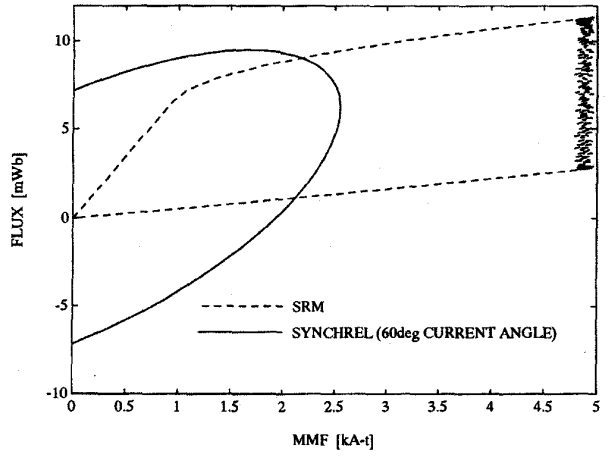

Fig. 9. Flux-MMF diagram for the SYNCHREL and SRM.

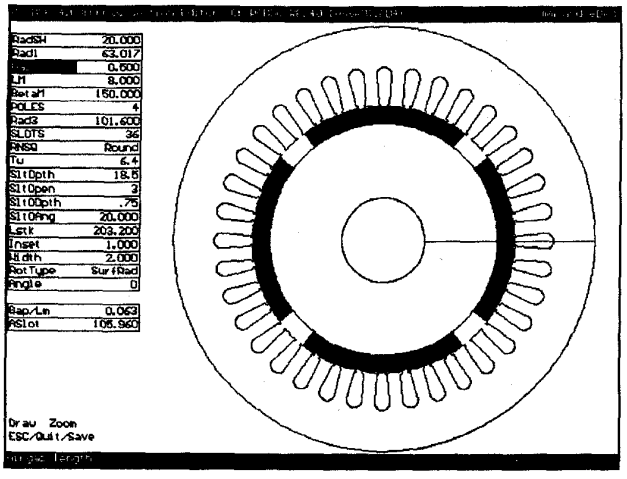

Fig. 10. SPM-AC and SPM-DC1 motor designs.

due to slotting (Fig. 13). A typical full-load flux plot taken from the finite-element analysis is shown in Fig. 11.

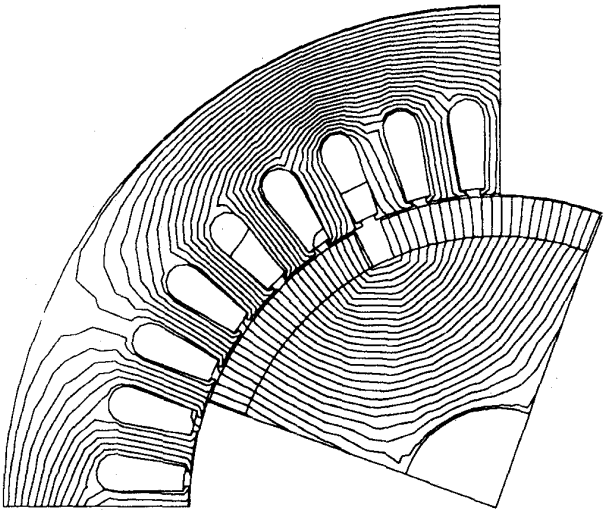

Fig. 11. SPM-AC flux plot (full-load, $\theta = 20°$).

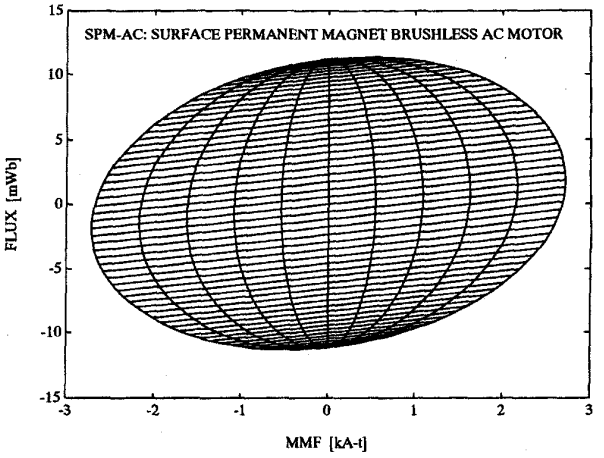

Fig. 12. flux-MMF diagram and magnetization curves for the SPM-AC motor (6 phase current values with the maximum at full-load).

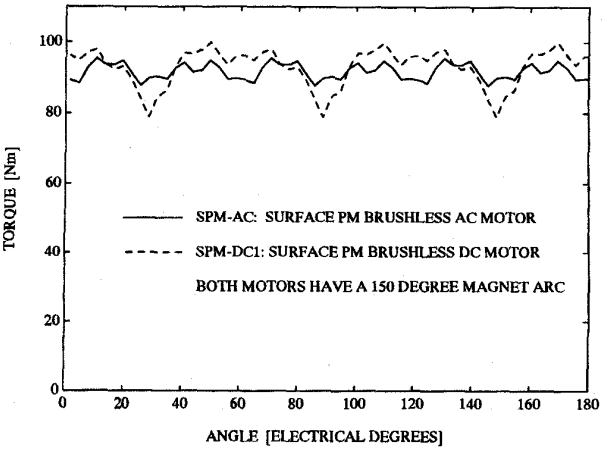

Fig. 13. SPM-AC and SPM-DC1 torque ripple (FE predication at full-load).

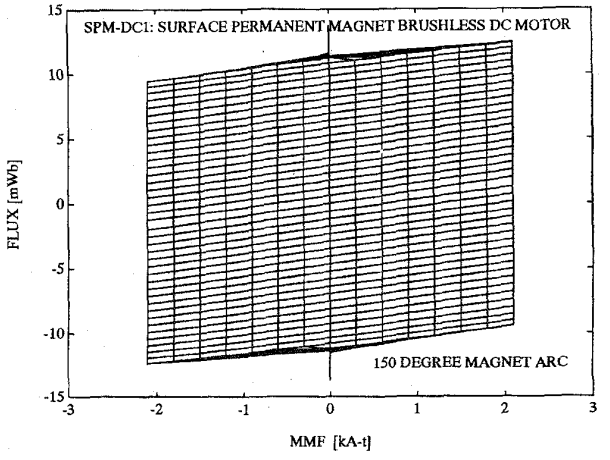

Fig. 14. Flux-MMF diagram and magnetization curves for the SPM-DC1 motor (8 phase current values with the maximum at full-load).

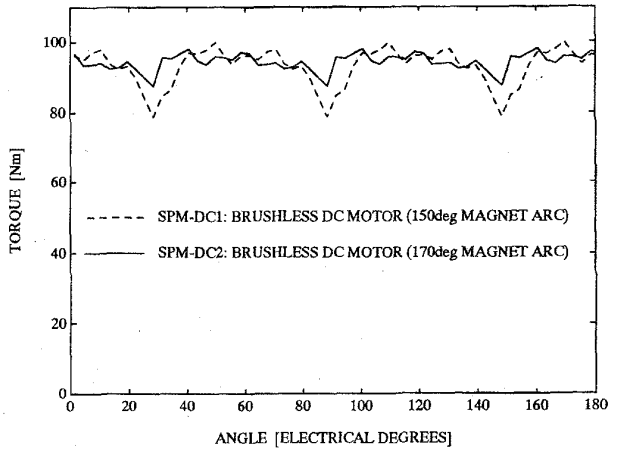

Fig. 15. SPM-DC1 and SPM-DC2 torque ripple (FE prediction at full-load).

E. Surface Permanent Magnet Brushless DC (SPM-DC)

Two surface permanent magnet brushless dc (SPM-DC) motors were designed to operate with 120° squarewave line currents:

1) SPM-DC1 with a 150° magnet arc: this uses the same geometry and magnets as the SPM-AC motor, with a concentrated winding to give a flat-top back-emf waveform.
2) SPM-DC2 with a 170° magnet arc: this motor is exactly the same as SPM-DC1 except that it uses a larger magnet arc to reduce the torque ripple.

Fig. 14 is the flux-MMF diagram for the SPM-DC1 motor. The diagram has a nearly ideal rectangular shape and regular spacing of the magnetization curves, with a small amount of torque ripple that is reduced in the SPM-DC2 design (Fig. 15).

F. Interior Permanent Magnet Motor (IPM)

The interior permanent magnet (IPM) motor was also designed using *PC-BDC*, Fig. 16. It was designed to operate from a sinusoidal supply and uses the same stator and winding as

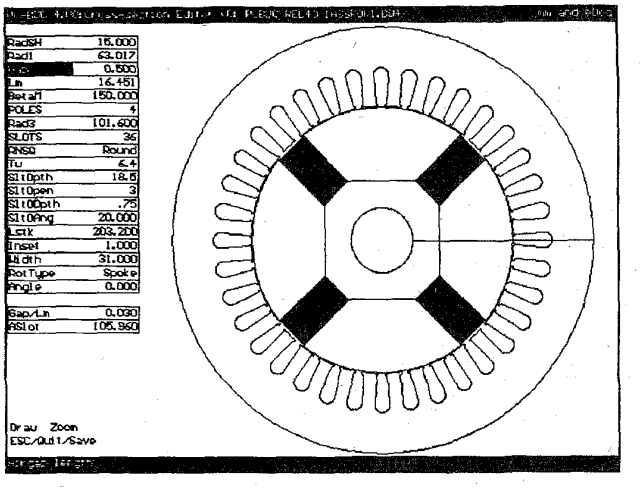

Fig. 16. IPM motor design.

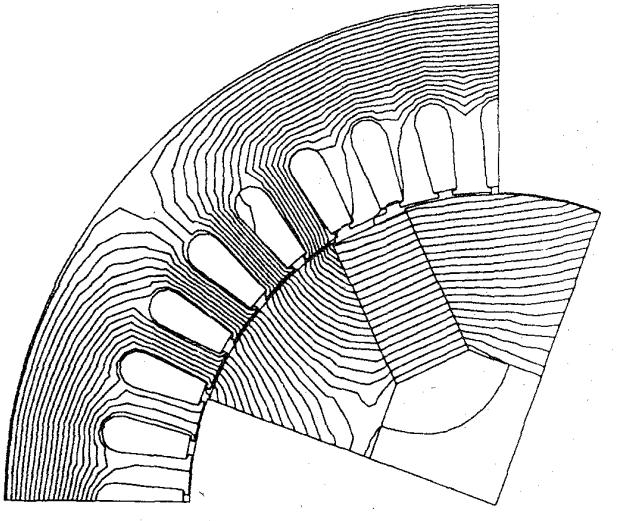

Fig. 17. IPM flux plot (full-load, $\theta = 20°$).

the SPM-AC motor. Fig. 18 is the flux-MMF diagram (with $\gamma = 30°$ selected for maximum torque/ampere). The contrast between flux-MMF diagrams for the SPM-AC and IPM motors is evident from Figs. 12 and 18, respectively. Although both motors have the same average torque, the deviation from the near ideal elliptical shape and uneven spacing of the magnetization curves indicate larger torque ripple in the IPM (Fig. 19). A typical full-load flux plot taken from the finite-element analysis is shown in Fig. 17.

G. Permanent Magnet DC Commutator Motor (PMDC)

The permanent magnet dc commutator motor (PMDC) used in the analysis is shown in Fig. 20. It was designed using the *PC-DCM* program [23]. It has the same numbers of slots and poles as the SPM-DC motor, resulting in a "9 phase" motor. The magnet has a remanence of 0.75 T. This is less than the 1.1 T used in the SPM-DC motor but is required to increase the copper space, noting the flux-concentration in PMDC motors. The flux-MMF diagram is shown in Fig. 22 and the predicted

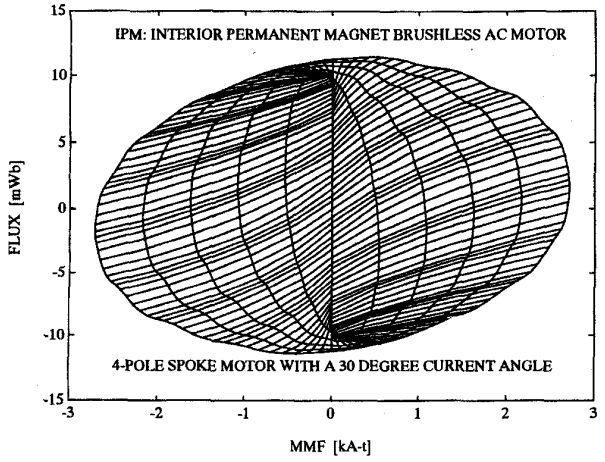

Fig. 18. Flux-MMF diagram and magnetization curves for the IPM motor (6 phase current values with the maximum at full-load).

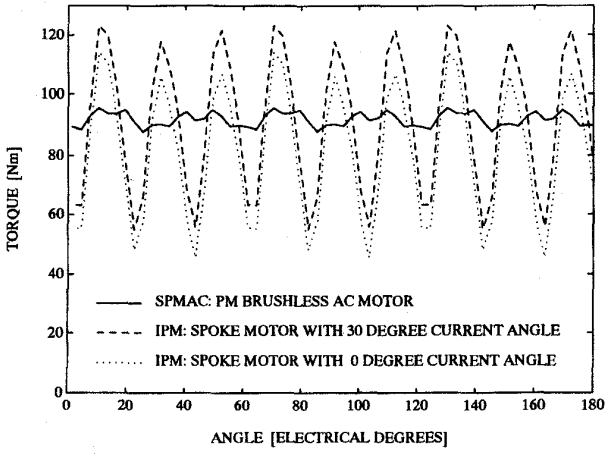

Fig. 19. SPM-AC and IPM torque ripple (FE prediction at full-load).

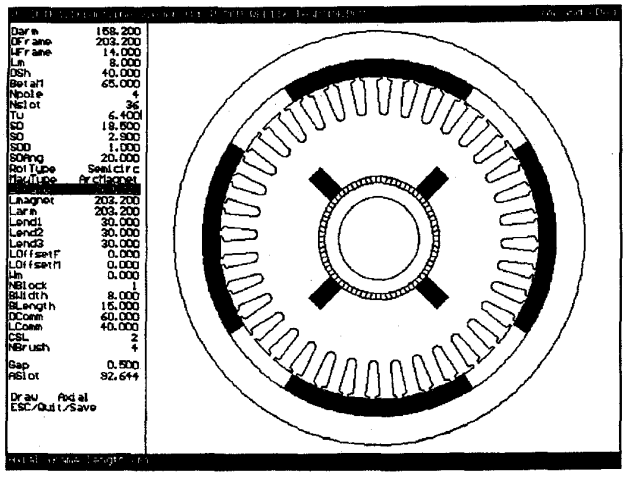

Fig. 20. PMDC motor design.

torque ripple in Fig. 23. A typical full-load flux plot taken from the finite-element analysis is shown in Fig. 21.

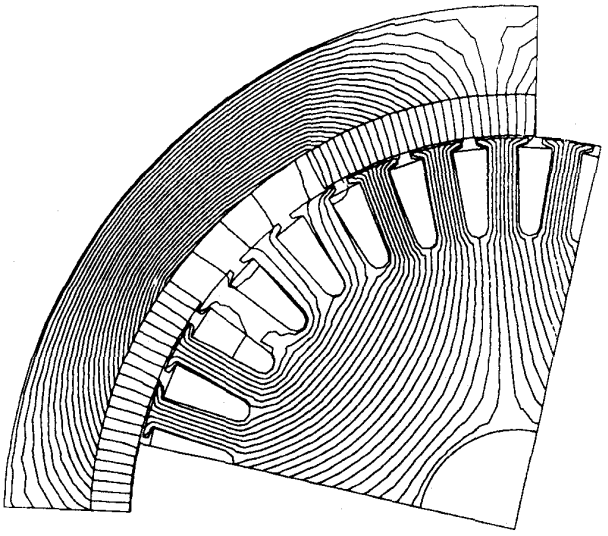

Fig. 21. PMDC flux plot (full-load, $\theta = 10°$).

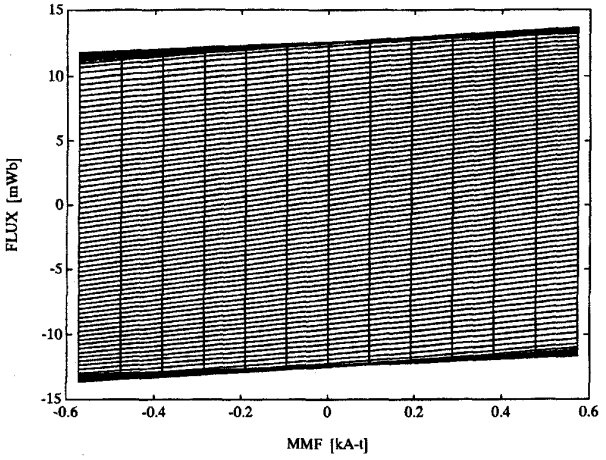

Fig. 22. Flux-MMF diagram and magnetization curves for the PMDC motor (6 values of current with the maximum at full-load).

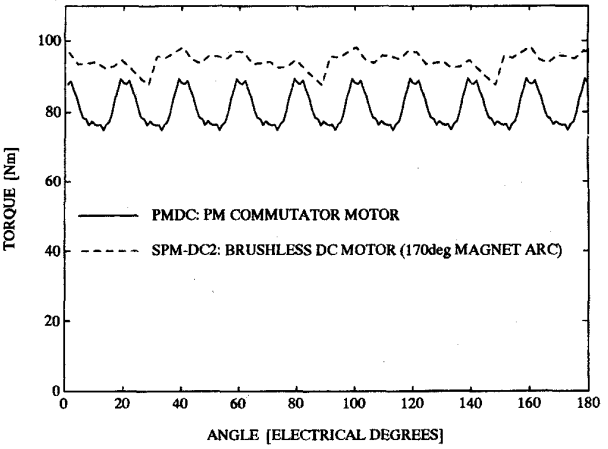

Fig. 23. Torque ripple in the PMDC and SPM-DC2 motors (full-load).

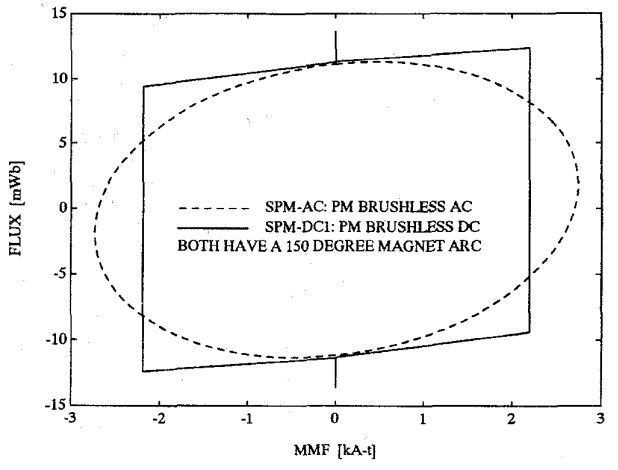

Fig. 24. Flux-MMF diagram for the SPM-AC and SPM-DC1 motors (full-load).

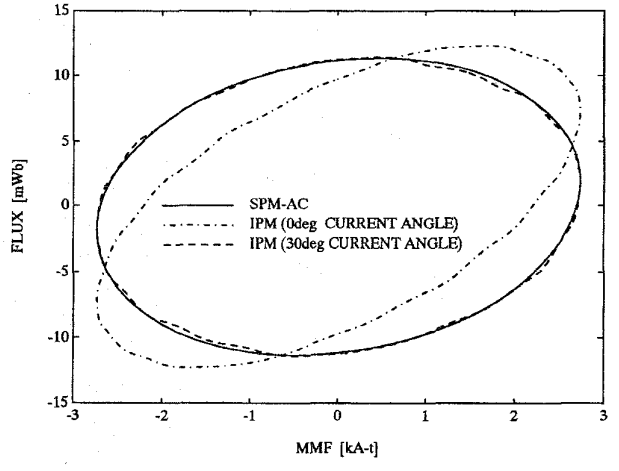

Fig. 25. Flux-MMF diagram for the SPM-AC and IPM motors (full-load).

V. Comparisons Based on the Flux-MMF Diagram

Table II and Figs. 26–29 compare average torque, torque ripple (expressed as the ratio of peak-peak to mean), peak phase MMF and peak effective phase flux for each motor type.

A. IM, SYNCHREL, and SPM-AC

Fig. 2 compares the IM, SYNCHREL, and SPM-AC motors. The maximum electric and magnetic loadings for the three motors are roughly comparable. However the SPM-AC motor can generate substantially more torque. The difference is due to the power-factor. The SPM-AC motor has close to unity power-factor while the other two motors have a lower value. The poor power factor is compounded in the case of the IM as it has been derated from 11 kW to 7.5 kW (Section IV-A). Thus the IM and SYNCHREL motors are being limited by their magnetizing current requirements. The SPM-AC motor requires no magnetizing current and so it can operate at a near unity power-factor, as is reflected by the near alignment between the major axis of the ellipse and the MMF axis (Fig. 12).

TABLE II
Comparison Between Motor Types

Motor	T_{AV} (Nm)	T_{RIPPLE} (%)	Peak MMF (kA-t)	Peak Flux (mWb)
IM	49.7	-	2.07	10.53
SYNCHREL	54.8	25	2.55	9.50
SRM	63.4	75	4.98	11.33
SPM-AC	91.7	8	2.74	11.32
SPM-DC1	93.0	23	2.19	13.6
SPM-DC2	94.2	11	2.19	13.98
IPM (γ=0°)	80.9	85	2.74	12.58
IPM (γ=30°)	91.3	75	2.74	11.62
PMDC	81.1	18	1.74[a]	13.62

[a] The peak phase MMF for the PMDC motor has been multipled by 3 as it is a "9-phase" motor (all the other motors have 3 phases)

B. SYNCHREL and SRM

Fig. 9 compares the SYNCHREL with the SRM. The SRM shows a similar flux level and much higher MMF. Torque is not dramatically better as the SRM is limited to the first quadrant while the SYNCHREL (and other ac motors) can benefit from mutual flux-linkage and so extend into the fourth quadrant. The SRM has high torque ripple, although no attempt has been made to reduce it in this design.

C. SPM-AC and SPM-DC

Fig. 24 compares the flux-MMF diagrams of the SPM-AC and SPM-DC1 motors. Both have almost the same area and average torque. However, the torque ripple is less in the SPM-AC motor. It is to be noted that the peak current rating of the inverter is higher with the sinusoidal drive. The peak flux in the SPM-DC motor is larger than in the SPM-AC motor (even when they have the same geometry and magnets), because the winding is concentrated rather than distributed.

SPM-DC2 has a 170° magnet arc to reduce the torque ripple to levels comparable with the SPM-AC motor. (This does not take account of imperfect commutation at higher speeds.)

D. SPM-AC and IPM

The IPM has almost the same torque as the SPM-AC motor, as reflected by equivalent ellipsoidal areas in Fig. 25. However, the torque ripple is much larger (Fig. 19). This is due to the uneven spacing of the magnetization curves shown in Fig. 18. The torque ripple is due to harmonics in the airgap permeance caused by slotting. The torque ripple can be minimized by skewing [24], which also reduces the cogging torque [10]. The IPM with $\gamma = 30°$ has a better power factor than with $\gamma = 0°$, as indicated by the orientation of the ellipses in Fig. 25.

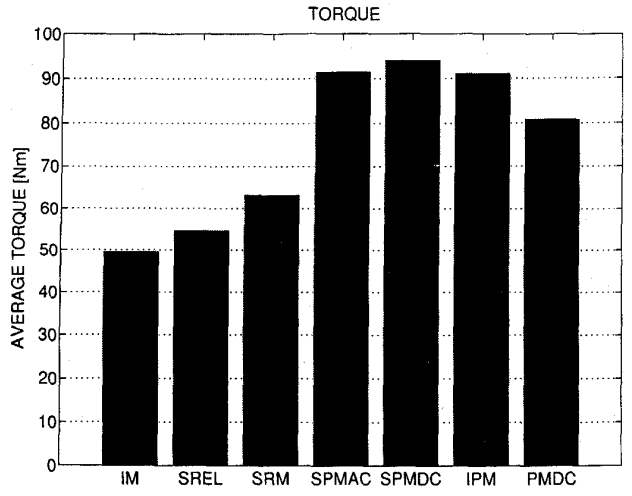

Fig. 26. Average rated torque in the 7 motors used in the comparison.

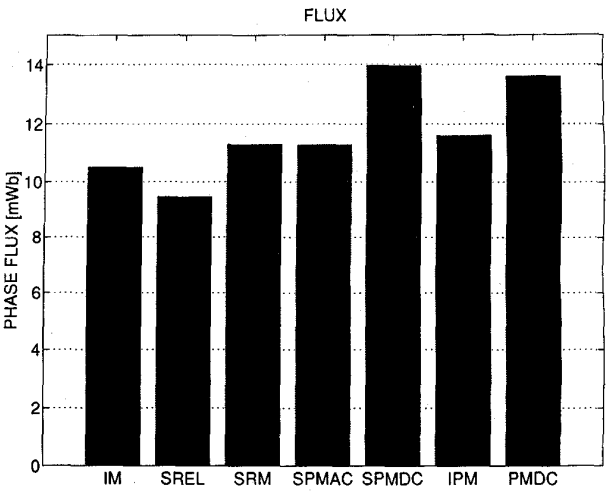

Fig. 28. Effective flux in the 7 motors used in the comparison.

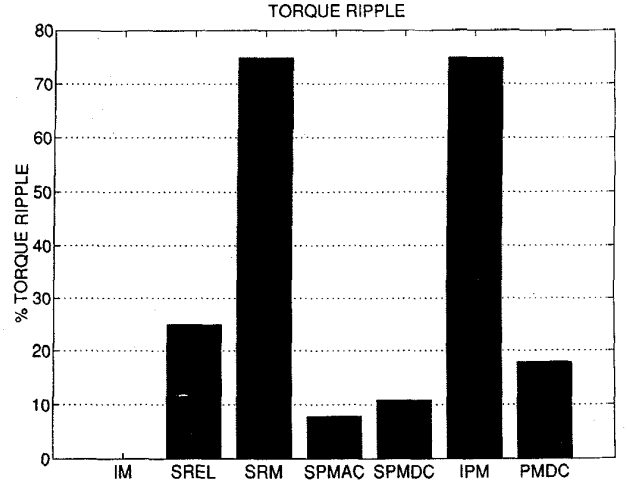

Fig. 27. Torque ripple in the 7 motors used in the comparison.

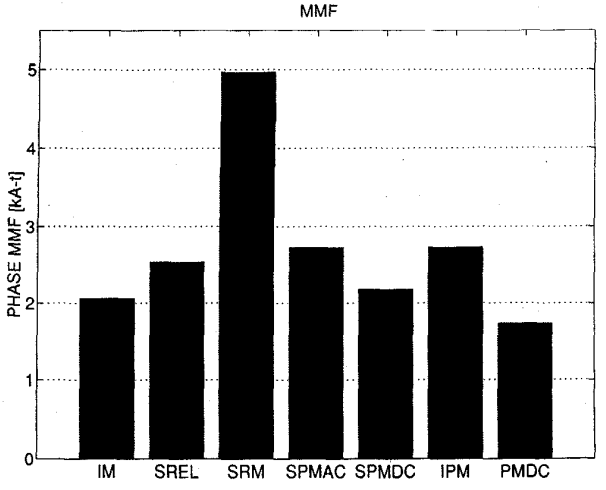

Fig. 29. MMF in the 7 motors used in the comparison.

E. SPM-DC and PMDC

The comparison between the SPM-DC and PMDC motors is complicated by the fact that they have different number of phases. This results in a low peak phase MMF in the PMDC motor. Even if the phase ratio (9/3) is used to scale MMF's, the PMDC motor has a smaller MMF. This is mainly due to the fact that the SPM-DC motor has its slots on the outside of the motor and has a greater winding area. Even though a lower grade magnet is used in the PMDC motor, the effective flux is the same as in the SPM-DC motor. This is mainly due to the larger rotor diameter in the PMDC motor.

The PMDC motor may need to be derated with respect to the other motors because most of the losses are generated in the armature which is not as easily cooled as when it is on the outside of the motor.

VI. Conclusions

The flux-MMF diagram is a general theoretical means for calculating and comparing the average and instantaneous torque of a range of electric motors of different types. The method goes far beyond the capability of "unified" or "generalized" machine theory:

- It can deal with motors that cannot be analyzed using traditional methods for example, the doubly-salient SRM and the squarewave brushless dc motor.
- It can calculate instantaneous as well as average torque.
- It can calculate cogging and electromagnetic torque [10].
- It makes direct use of finite-element calculations in a way that is not possible with generalized-machine or "lumped-parameter" theories, and presents many of its results via graphical images whose features are readily associated with particular characteristics such as torque per unit volume, kVA requirement, torque ripple, etc.
- Because it is based on co-energy calculations and nonlinear magnetization data, the method is not restricted by assumptions of linearity or sinusoidal MMF distributions.

It would be unwise to proclaim the method as a modern-day replacement for generalized machine theory, which will

surely always be the foundation theory for ac and dc machines as well as for field-oriented control and some aspects of power-systems analysis; but it should help in the analysis and comparative evaluation of a wide range of electrical machines including new arrivals that fit no classical model.

REFERENCES

[1] T. J .E. Miller, *Switched Reluctance Motors and Their Control*. Oxford: Magna Physics Publishing and Oxford University Press, 1993.

[2] ——, *Brushless Permanent-Magnet and Reluctance Motor Drives*. Oxford: Oxford University Press, 1989.

[3] T. J. E. Miller and M. I. McGilp, "Nonlinear theory of the switched reluctance motor for rapid computer-aided design," in *IEE Proc.-B*, vol. 137, no. 6, Nov. 1990.

[4] F. Liang, Y. Liao, and T. A. Lipo, "A new variable reluctance motor utilizing an auxiliary commutation winding," *IEEE Trans. Ind. Applicat.*, vol. 30, no. 2, March/April 1994.

[5] D. A. Staton, W. L. Soong, and T. J. E. Miller, "Unified theory of torque production in switched reluctance and synchronous reluctance motors," *IEEE Trans. Ind. Applicat.*, vol. 31, no. 2, March/April 1995.

[6] Y. Liao, F. Liang, and T. A. Lipo, "A novel permanent magnet motor with doubly salient structure," in *Conf. Rec. IEEE-IAS Annu. Meeting*, Houston, Oct. 1992.

[7] H. H. Woodson and E. Melchen, *Electromechanical Dynamics*. New York: Wiley, 1968.

[8] D. C. White and H. H. Woodson, *Electromechanical Energy Conversion*. New York: Wiley, 1959.

[9] A. E. Fitzgerald and J. R. Kingsley, *Electrical Machinery*, 2nd Ed. New York: McGraw-Hill, 1961.

[10] R. P. Deodhar, D. A. Staton, T. M. Jahns, and T. J. E. Miller, "Prediction of cogging torque using the flux-MMF diagram technique," in *Conf. Rec. IEEE-IAS Annu. Meeting*, Orlando, FL, Oct. 1995.

[11] D. A. Staton, T. J. E. Miller, and S. E. Wood, "Maximising the saliency ratio of the synchronous reluctance motor," in *IEE Proc. B*, vol.140, no. 4, July 1993, pp. 249–259.

[12] L. Xu, X. Xu, T. A. Lipo, and D. W. Novotny, "Control of a synchronous reluctance motor including saturation and iron loss," *IEEE Trans. Ind. Applicat.*, vol. 27, no. 5, pp. 977–985, Sept/Oct. 1991.

[13] I. Boldea, Z. X. Fu, and S. A. Nasar, "Performance evaluation of axially laminated anisotropic (ALA) rotor reluctance synchronous motors," *IEEE Trans. Ind. Applicat.*, vol. 30, no. 4, July/August 1994.

[14] A. J. O. Cruickshank, A. F. Anderson, and R. W. Menzies, "Theory and performances of reluctance motors with axially laminated anisotropic rotors," in *Proc. IEE*, vol. 118, no. 7, 1971.

[15] D. Platt, "Reluctance motor with strong anisotropy," in *Conf. Rec. IEEE-IAS Annu. Meeting*, Seattle, WA, Oct. 1990, pp. 225–229.

[16] A. Fratta and A. Vagati, "Axially laminated reluctance motor: An analytical approach to the magnetic behaviour," in *Int. Conf. Elec. Mach.*, Pisa, Italy, vol. III, Sept. 1988, pp. 1–6.

[17] T. A. Lipo, A. Vagati, L. Malesani and T. Fukao, "Synchronous reluctance motors and drives—A new alternative," in *IEEE-IAS Annu. Meeting*, Houston, Oct. 1992.

[18] A. Vagati and T. A. Lipo, "Synchronous reluctance motors and drives—A new alternative," in *IEEE-IAS Annu. Meeting*, Denver, Oct. 1994.

[19] R. E. Betz and T. J. E. Miller, "Aspects of the control of synchronous reluctance machines," in *European Power Electron. Conf., EPE91*, Florence, Sept. 1991.

[20] W. L. Soong, D. A. Staton, and T. J. E. Miller, "Design of a new axially-laminated interior permanent magnet motor," *IEEE Trans. Ind. Applicat.*, vol. 31, no. 2, March/April 1995.

[21] J. R. Hendershot and T. J. E. Miller, *Design of brushless permanent-magnet motors*. Oxford: Magna Physics Publishing and Oxford University Press, 1994.

[22] D. A. Staton, M. I. McGilp, T. J. E. Miller, and G. Gray, "High-speed PC-based CAD for motor drives," in *5th EPE Conf.*, Brighton, Sept. 1993.

[23] D. A. Staton, T. J. E. Miller, and M. I. McGilp, "Interactive computer aided design of permanent magnet DC motors," in *Conf. Rec. IEEE-IAS Annu. Meeting*, Toronto, Canada, Oct. 1993.

[24] R. P. Deodhar, D. A. Staton, and T. J. E. Miller, "Modelling of skew using the flux-MMF diagram," *IEEE-PEDES Conf.*, New Delhi, India, Jan. 1996, in press.

David A. Staton was born in Chesterfield, England, on July 29, 1961. He received the B.Sc. (Hons.) degree in electrical and electronic engineering from Trent Polytechnic, Nottingham, England, in 1983 and the Ph.D. degree from the University of Sheffield, England, in 1988.

From 1977 to 1984, he was employed by British Coal, who sponsored him while he was undertaking the B.Sc. degree. While at the University of Sheffield, he developed CAD software for permanent-magnet dc motors in collaboration with GEC Electromotors Ltd. From 1988 to 1989, he was with Thorn EMI Central Research Laboratories and was engaged in the design of motors for the Kenwood range of food processors. From 1989 to 1995, he was employed as a research assistant in the SPEED Laboratory at the University of Glasgow. Presently he is with Control Techniques plc, Newtown, Wales. His research interests are in the computer aided design of permanent-magnet and reluctance motors.

Rajesh P. Deodhar (S'88–M'90–S'94) was born in Bombay, India, on February 22, 1968. He received the Bachelor of Engineering (B.Eng.) degree in electronics engineering from the University of Bombay in 1989 and the Master of Technology (M.Tech.) degree in electronic product design from the Center for Electronic Design and Technology (CEDT) at the Indian Institute of Science, Bangalore, in 1991. Since the beginning of 1994, he has been working towards the Ph.D. degree in the SPEED Laboratory, University of Glasgow, Scotland, in the generalized area of design and analysis of electric machines and drives.

From 1991 to 1993, he worked as a Design Engineer with Crompton Greaves Ltd., Bombay, on the design of induction and brushless PM motors and drives. In 1993 he spent six months in Japan, working with Hitachi Ltd., on the applications of electric machines and drives in home appliances.

Mr. Deodhar was awarded the CEDT Design Gold Medal by the Indian Institute of Science in 1991. He also received the Hitachi-AOTS scholarship in 1993 which enabled him to work with Hitachi Ltd. in Japan for six months. He is an Associate Member of the IEE, U.K.

Wen L. Soong (S'89–M'90–S'90–M'93) was born in Kuala Lampur, Malayasia, and received the B.Eng. degree from Adelaide University, Australia, in 1989, and the Ph.D. degree from Glasgow University, Scotland, in 1993.

He is an electrical engineer in the Power Controls Programs at General Electric Corporate Research and Development, Schenectady, NY. His research interests include permanent magnet and reluctance motor design and modeling, field-weakening control, and sensorless control.

Timothy J. E. Miller (M'74–SM'82) is a native of Wigan, U.K. He was educated at Atlantic College, the University of Glasgow, Scotland, and the University of Leeds.

From 1979 to 1986 he was an electrical engineer and program manager at General Electric Corporate Research and Development, Schenectady, NY. His industrial experience includes periods with GEC (U.K.), British Gas, International Research and Development, and a student-apprenticeship with Tube Investments Ltd. He is Lucas Professor in Power Electronics, and founder and Director of the SPEED Consortium at the University of Glasgow, Scotland. He is the author of 105 publications in the fields of motors, drives, power systems, and power electronics.

Prof. Miller is a Fellow of the Royal Society of Edinburgh and a Fellow of the IEE.